Available online at www.sciencedirect.com
ScienceDirect
ELSEVIER
Applied Surface Science 253 (2006) 2915–2923
applied surface science
www.elsevier.com/locate/apsusc

Temperature and N^+ energy dependence on nano-structural modifications and characteristics of Mo surface

H. Savaloni [a,b,*], M. Motmaen-Dadgar [b], M. Ghoranneviss [b], M.R. Hantehzadeh [b]

[a] Department of Physics, University of Tehran, North-Kargar St., Tehran, Iran
[b] Plasma Physics Research Center, Science and Research Campus of Islamic A. University, P.O. Box 14665-678, Tehran, Iran

Received 5 March 2006; received in revised form 6 June 2006; accepted 6 June 2006
Available online 18 July 2006

Abstract

The surface modifications of Mo massive samples (0.5 mm foils) made by nitrogen ion implantation are studied by SEM, XRD, AFM, and SIMS. Nitrogen ions in the energy range of 16–30 keV with a fluence of 1×10^{18} N^+ cm^{-2} were implanted in molybdenum samples for 1600 s at different temperatures. XRD patterns clearly showed MoN (0 3 1) (hcp) very close to Mo (2 0 0) line. Crystallite sizes (coherently diffracting domains) obtained from MoN (0 3 1) line, showed an increase with substrate temperature. AFM images showed the formation of grains on Mo samples, which grew in size with temperature. Similar morphological changes to that has been observed for thin films by increasing substrate temperature (i.e., structure zone model (SZM)), is obtained. The density of implanted nitrogen ions and the depth of nitrogen ion implantation in Mo studied by SIMS showed a minimum for N^+ density as well as a minimum for penetration depth of N^+ ions in Mo at certain temperatures, which are both consistent with XRD results (i.e., $I_{Mo\ (2\ 0\ 0)}/I_{Mo\ (2\ 1\ 1)}$) for Mo (bcc). Hence, showing a correlation between XRD and SIMS results. This phenomenon is explained on the basis of residual gas, substrate temperature, dissociation of water in the chamber and the ion energy.
© 2006 Elsevier B.V. All rights reserved.

Keywords: SEM; AFM; XRD; SIMS; Ion implantation; Depth profile; Molybdenum

1. Introduction

In our earlier work [1] we reported the influence of N^+ implantation in tungsten (one of the two elements (W and Mo) which are the most difficult materials to form nitride [2], because they show the lowest reactivity with nitrogen and the respective compounds, the lowest stability and the narrowest region of existence in the phase diagrams [3,4]) as a function of temperature and N^+ energy. This paper is an extension of our work to molybdenum.

Molybdenum nitride and tungsten nitride play a significant role in the development of new catalytic systems for obtaining higher thermal resistance properties with respect to the conventional catalytic systems based on supported Ni–Mo and CoMo sulfides [5–7].

The aim of this article is to investigate the nature of nitride formation in molybdenum during nitrogen implantation, as a function of substrate temperature and N^+ ion energy.

2. Experimental details

The samples used were cut in two different sizes of 3 mm × 3 mm (for SIMS analysis), 10 mm × 5 mm (for XRD, SEM and AFM analysis) from 0.5 mm thick polycrystalline Mo foil (Balzers; No. 07050). Neither mechanical nor chemical polishing treatments were applied to the samples' surfaces. The r.m.s. surface roughness R_{rms} and R_{av} of Mo surface was measured by AFM.

The nitrogen ion implantation of the samples was carried out at 16–30 keV and a fluence of 1×10^{18} N^+ cm^{-2} with a current density of 100 $\mu A\ cm^{-2}$ for 1600 s. The base pressure of the chamber was 2×10^{-5} mbar, which during the implantation process increased to 6×10^{-5} mbar.

A substrate holder system with controlled heating system was designed and constructed. Detailed description of this is given in our earlier work [8]. On the copper disk substrate holder two of

* Corresponding author. Tel.: +98 21 88635776; fax: +98 21 88004781.
E-mail address: savaloni@khayam.ut.ac.ir (H. Savaloni).

0169-4332/$ – see front matter © 2006 Elsevier B.V. All rights reserved.
doi:10.1016/j.apsusc.2006.06.035

Table 1
Details of molybdenum samples investigated

Sample no.	N^+ energy (keV)	Initial temperature, T_{si} (K)	Final temperature, T_{sf} (K)	$d_{MoN\ (0\ 3\ 1)}$ (Å)	$d_{MoO_2 (1\ 1\ 3)}$ (Å)	D (Å)
Mo	Untreated	RT	RT	–	–	–
Mo1	Group I	300	673	1.5788	1.2874	140
Mo2		423	695	1.5782	1.2868	450
Mo3		523	722	1.5759	1.2850	570
Mo4		623	741	1.5762	1.2859	770
Mo5	Group II	300	698	1.5785	1.2885	220
Mo6		423	725	1.5772	1.2883	650
Mo7		523	752	1.5766	1.2865	900
Mo8		623	777	1.5772	1.2863	810
Mo9	Group III	300	730	1.5772	1.2878	240
Mo10		423	750	1.5782	1.2876	620
Mo11		523	778	1.5779	1.2972	1000
Mo12		623	801	1.5766	1.2857	830
Mo13	Group IV	300	753	1.5785	1.2872	240
Mo14		423	772	1.5759	1.2863	890
Mo15		523	800	1.5779	1.2861	890
Mo16		623	833	1.5762	1.2863	1000

Group I: 16 keV; group II: 20 keV; group III: 25 keV; group IV: 30 keV. D: crystallite size (coherently diffracting domains).

each size of the substrates can be fixed by a stainless steel mask. The substrate temperatures were controlled by programmed thermostats and thermocouples fixed inside a hole on the surface of copper disk substrate holder.

Just before use all Mo samples were ultrasonically cleaned in heated acetone then ethanol.

The crystallographic structure of the samples was obtained using a PTS 3003 Diffractometer, while the surface physical morphology and roughness was obtained by means of AFM (Park Scientific) analysis as well as SEM. The density of implanted N^+ ions in Mo samples as well as depth profiling was carried out, using SIMS (Cameca, IMS 6F) analysis. Cs^+ ions were used as primary ions with +5 keV impact energy on the surface of the sample and positive secondary ions (N^+) were detected. The spot size for SIMS measurements was 5 μm. Prior to each real sample analysis the stability of the ion source was checked and during the process of SIMS analysis of each sample, in addition to the depth profile analysis of N^+, the Cs^+Mo^+ and Mo^+ were also analyzed and no instability in the ion source was observed. The details of Mo samples produced for investigation in this work, and the data obtained from different analysis are given in Table 1.

3. Results

3.1. SIMS depth profile analysis and X-ray diffraction (XRD)

The distribution of N^+ ions of 16, 20, 25 and 30 keV implanted in Mo foils was simulated using SRIM2000 code. The nominal N^+ ion average projected range (R_p), straggling (ΔR_p), maximum/peak nitrogen concentration (C_p) and the expected sputtering rate (R_s) at the end of implantation process (i.e., after 60,000 ions implanted), obtained from SRIM2000 calculations are given in Table 2. With respect to the results of the sputtering rate it should be noted that since the binding energy of the surface atoms for molybdenum is not available, the heat of sublimation is used instead in the SRIM calculation, which apparently does not predict the realistic values and should be considered as a rough estimate. It should also be noted that the role of temperature, ion flounce and some other parameters such as surface roughening, hence change of surface binding energy are not included in SRIM2000 computer simulation code.

The SIMS nitrogen profile of implanted Mo at four different energies of 16, 20, 25 and 30 keV and for four different temperatures are given in Fig. 1(a)–(d). It should be mentioned that the initial temperature (T_{si}) which is given in column 3 of Table 1, was set before implantation and it changed during implantation process owing to heat transfer from ion beam to the samples. The final temperature of the samples (T_{sf}) at the end of implantation process is given in column 4 of Table 1 and as a typical example, the progress of temperature during implantation of 20 keV N^+ ions with time for four different initial temperatures (group II in Table 1) is given in Fig. 2, similar to our earlier work on tungsten samples. The data were analyzed according to this final temperature, as in fact this temperature effectively acts on the activated processes in the sample, until the sample cools down to room temperature in

Table 2
Data obtained from SRIM2000 simulation

N^+ energy (keV)	R_p (nm)	ΔR_p (nm)	C_p (atoms/cm^3)	R_s (atoms/ion)
16	21.7	11.7	2.5×10^{23}	0.8887
20	26.1	13.9	2.2×10^{23}	0.8562
25	31.5	16.5	1.9×10^{23}	0.7828
30	37.0	19.0	1.65×10^{23}	0.7631

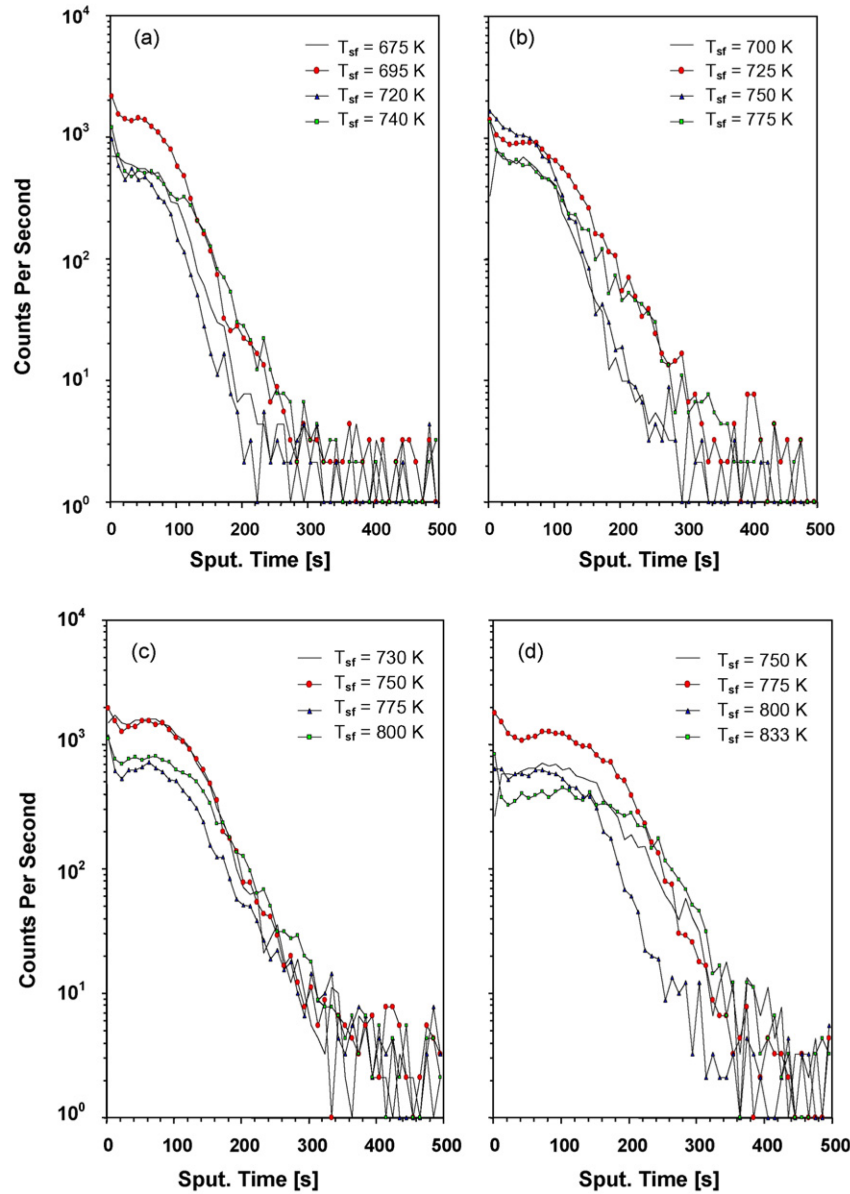

Fig. 1. N^+ ion SIMS profiles of implanted Mo at different energies. (a) 16 keV; (b) 20 keV; (c) 25 keV; (d) 30 keV.

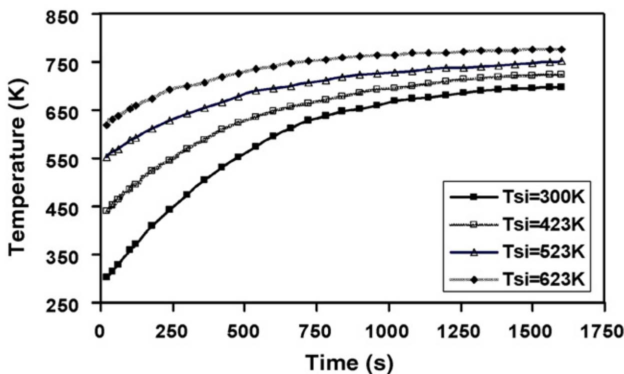

Fig. 2. The progress of Mo foil temperature during N^+ ion implantation of 20 keV energy for different initial energies.

vacuum (which took 3–5 h depending on the final temperature). It is well known that the change of temperature during implantation can play a role in the nucleation and post nucleation stages of the surface modification. However, we could not take this into account, and on the other hand in most cases did not change dramatically. In Fig. 2, it can be observed that the time required to reach almost the final temperature for all initial temperatures is about 800 s (i.e., one half of the implantation time). This is similar to our work on tungsten [1].

The SIMS profiles obtained may be analyzed in two ways, shown in Fig. 3(a) and (b). The area under each curve, peculiar to each temperature was obtained, as a measure of the amount (density) of the implanted nitrogen ions in Mo samples (Fig. 3(a)). The results show that, the N^+ density decreases to a

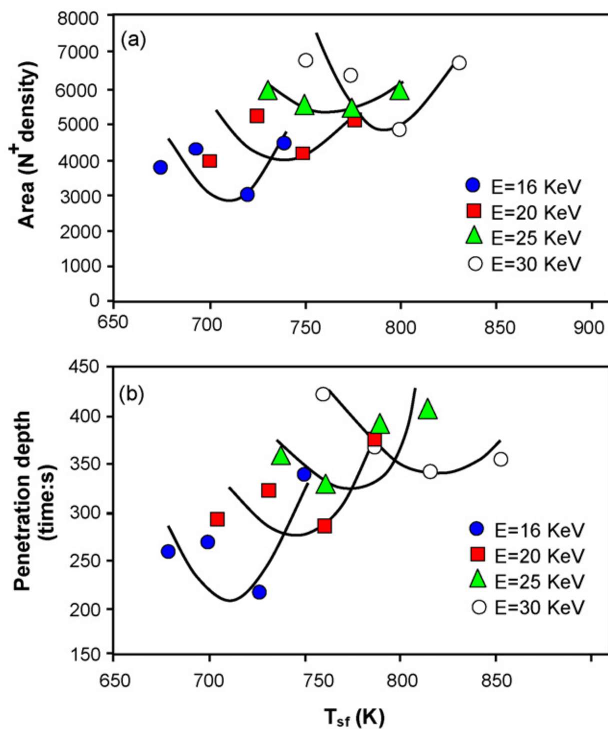

Fig. 3. (a) N^+ ions density and (b) penetration depth of N^+ ions in Mo vs. final temperature for different N^+ ion energies.

minimum with increasing the temperature, and further increase of temperature increases the N^+ density. Similar behavior can be observed in the penetration depth of N^+ in Mo samples (Fig. 3(b)). The size of the symbols in these figures is chosen so that they are larger than the uncertainties. In addition the curves fitted to the data are used as a guide for the eye. The behavior of the results for both N^+ density (Fig. 3(a)) and penetration depth (Fig. 3(b)) is consistent with those obtained for N^+ implanted W [1]. Ideally, in order to investigate the penetration depth quantitatively, the sputtering time should be converted to depth. This requires some means of measurement of the depth of the crater formed, such as large scan AFM or a suitable profilometer. Unfortunately, we did not have access to such instruments, hence the results presented here can be considered as qualitative information.

Fig. 4(a)–(d) shows the X-ray diffraction patterns obtained from untreated Mo, and those of N^+ implanted Mo at four different temperatures and four different N^+ energies (i.e., 16, 20, 25, and 30 keV).

The comparison of the XRD patterns (i)–(v) in Fig. 4(a)–(d), clearly shows the formation of MoN (0 3 1) (hexagonal) (JCPDS card No: 77-1999) and MoO_2 (1 1 3) (monoclinic) (JCPDS card No: 05-0452) lines very close to Mo (2 0 0) (bcc) and Mo (2 1 1) (bcc) (JCPDS card No: 42-1120) lines, respectively. The *d*-spacings of these lines obtained from the XRD patterns are listed in columns 5 and 6 of Table 1, respectively. In order to resolve the MoN (0 3 1) peak from Mo (2 0 0) peak and MoO_2 (1 1 3) peak from Mo (2 1 1), in each case two Voigt's functions plus a level background were fitted to the experimental peaks [9]. Typical examples of this are given in Fig. 5(a) and (b).

Fig. 6(a) and (b) shows the variation of the intensity of MoN (0 3 1) line for four different N^+ energies as a function of temperature and for four different temperatures as a function of N^+ energy, respectively. In Fig. 6(a) a minimum can be observed in the results of each N^+ energy. This minimum is similar to our results obtained on N^+ implanted W samples [1], confirming that there is a critical temperature for N^+ implantation process in which the reflected X-ray's intensity for metal nitrides formed (i.e., W and Mo) becomes minimum. In Ref. [1] the cause of this phenomenon in W implanted with N^+ ions is explained on the bases of the residual gas, substrate

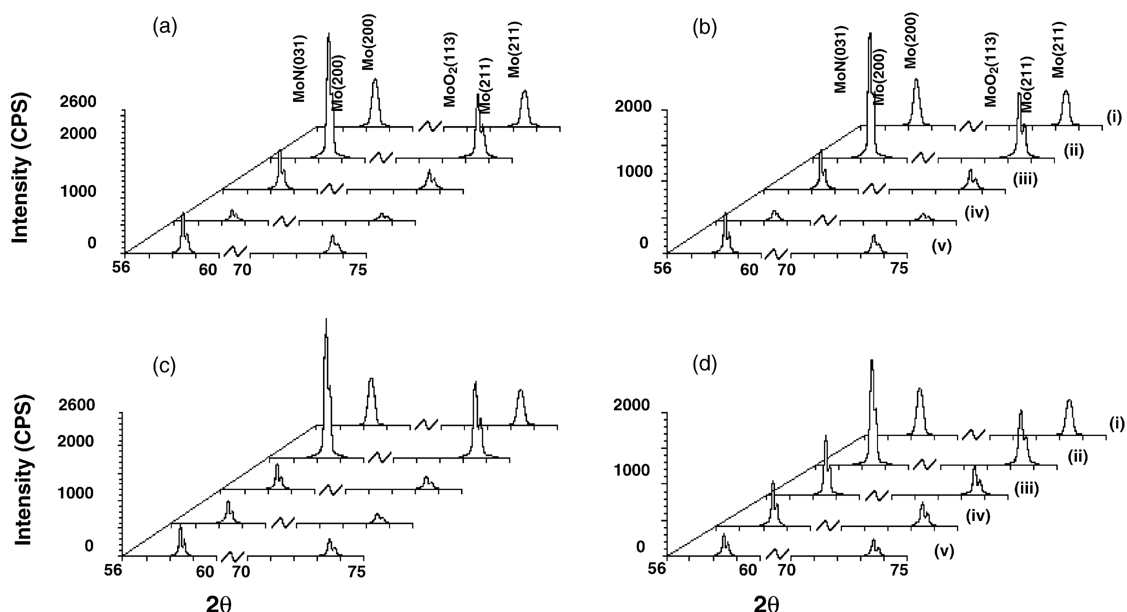

Fig. 4. XRD patterns obtained from N^+ ion implanted Mo samples at different N^+ energies. (a) 16 keV; (b) 20 keV; (c) 25 keV; (d) 30 keV. In (a–d) (i) stands for the untreated sample and (ii–v) are the results of different temperatures (T_{sf}) given in Table 1, in increasing order.

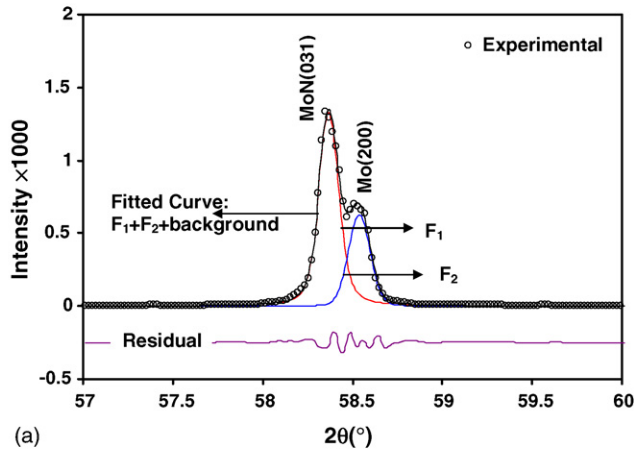

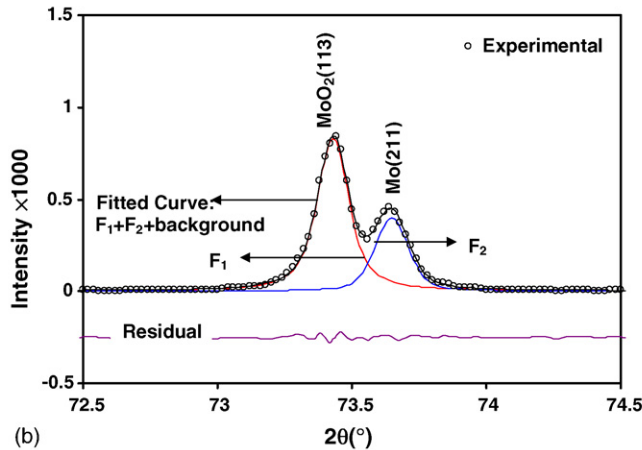

Fig. 5. (a) XRD peaks of MoN (0 3 1) and Mo (2 0 0) obtained for 20 keV N^+ ions implanted in Mo sample, fitted to two Voigt's functions and a level background. (b) XRD peaks of MoO_2 (1 1 3) and Mo (2 1 1) obtained for 20 keV N^+ ions implanted in Mo sample, fitted to two Voigt's functions and a level background.

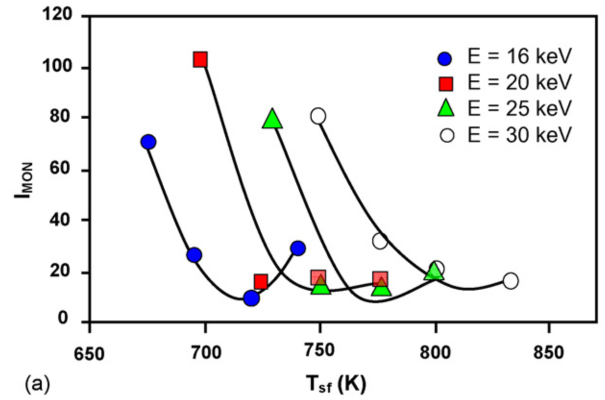

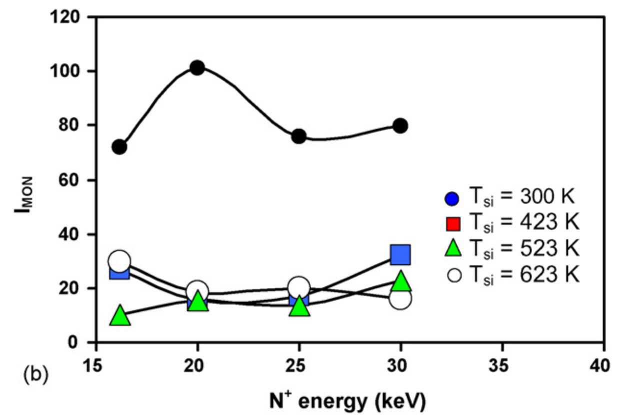

Fig. 6. (a) The intensity of MoN line as a function of final temperature for different N^+ energies. (b) The intensity of MoN line as a function of N^+ energy for different final temperatures.

temperature, dissociation of water in the chamber and the ion energy. This will be further discussed below.

Since in the XRD results of this work only MoN (0 3 1) line is observed, therefore it should be of interest to investigate the influence of N^+ implantation on the variation of Mo diffraction lines used in this work. Although, apparently the ratio of $I_{Mo\ (2\ 0\ 0)}/I_{Mo\ (2\ 1\ 1)}$ may not directly be relevant to this work but in fact the changes in this ratio has occurred after the ion implantation in the samples and to find a correlation between these two processes it could be of interest.

The intensity ratio of $I_{Mo\ (2\ 0\ 0)}/I_{Mo\ (2\ 1\ 1)}$ as a function of temperature and N^+ energy are shown in Fig. 7(a) and (b), respectively. In Fig. 7(a) a minimum for each N^+ energy is obtained, while in Fig. 7(b), apart from the data obtained for T_{si} = 523 K, there exist a minimum at 20 keV N^+ energy for three other temperatures. The minimums in Fig. 7(a) occur at the same temperature as those for the $I_{MoN\ (0\ 3\ 1)}$ in Fig. 6(a) and for corresponding energies. A same minimum as that in Fig. 7(b) was obtained for N^+ implanted W samples though at higher energy of 25 keV [1]. This can be due to higher density, melting point and hardness of tungsten. The minimums obtained in Fig. 7(a) are similar to the $I_{(1\ 1\ 1)}/I_{(2\ 0\ 0)}$ ratios obtained by Shi and Player [10] for Ni/SiO_2 thin films and by Savaloni et al. in sputtered Cu/glass thin films [11] and in Ag/glass films produced by electron beam under UHV condition [12]. The results of this work and N^+ implanted W [1] show the minimum at somewhat lower reduced temperatures ($T_s/T_m \sim 0.24$–0.26) and ($T_s/T_m \sim 0.18$–0.2), respectively, than that obtained for above thin films (i.e., $T_s/T_m \sim 0.28$–0.3). In our earlier work on N^+ implanted W, we pointed out that this may be due to three factors: (a) the different natures of the samples used, namely thin films and nitrogen ion implanted massive samples, (b) in the above cited references the intensity ratio for two associated lines (i.e., for example in the case of Ni, Cu or Ag (all fcc metals) the intensity ratio of $I_{(1\ 1\ 1)}/I_{(2\ 0\ 0)}$ is examined) is obtained, while in N^+ ion implanted works (i.e., W (bcc) and Mo (bcc)) (2 0 0) line is not directly associated with (2 1 1) line and (c) different crystallography structures (i.e., fcc compared to bcc).

The difference in this reduced temperature ratio (i.e., T_s/T_m) for N^+ implanted W ($T_s/T_m \sim 0.18$–0.2) and N^+ implanted Mo ($T_s/T_m \sim 0.24$–0.26) could be due to the lower melting point of Mo compared to that of W. Therefore, more processes become activated in Mo under similar temperature (in this work, T_{si} was set at the same temperature as that used in our earlier work on W [1], while the same system was also used) and N^+ energy than those for W sample (e.g., higher surface and bulk diffusions may take place. Hence grains' structure will change accordingly).

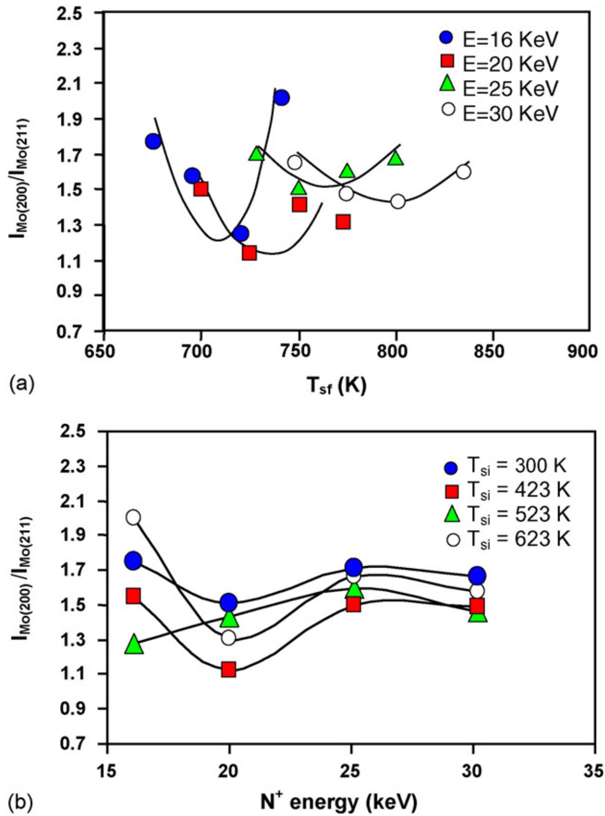

Fig. 7. (a) The intensity ratio of Mo (2 0 0)/Mo (2 1 1) as a function of final temperature for different N^+ energies. (b) The intensity ratio of Mo (2 0 0)/Mo (2 1 1) as a function of N^+ energy for different final temperatures.

This phenomenon (i.e., occurrence of minimum in the plot of X-ray diffraction intensity ratio for two lines versus reduced temperature) has not been explained in case of thin films, so far. The Walton's model [13] (based on the stability of the critical nuclei, the structure of which determines the orientation of the film) to explain the increased intensity ratio at lower temperature than the minimum, and Lee's model [14] (in which planes with higher surface energy are favored at higher temperature because they have more ledges) for higher temperatures than this minimum are not capable of explaining this phenomenon. Therefore the occurrence of the minimum remains unexplained, and it can be more complex in the case of nitrogen ion implanted Mo and W, though for the latter an explanation is given in our earlier work [1], which should also be valid for Mo.

The minimums obtained in the results of SIMS for the density of the implanted nitrogen ions in Mo (Fig. 3(a)) and for the penetration depth of N^+ ions in Mo (Fig. 3(b)), and the minimums obtained in analyzing XRD results (i.e., Fig. 5(a) for $I_{MoN\ (0\ 3\ 1)}$ and Fig. 7(a) for $I_{Mo\ (2\ 0\ 0)}/I_{Mo\ (2\ 1\ 1)}$) occur at the same temperature and shows a clear correlation between the results obtained from XRD and SIMS, while as discussed above, the similar XRD results (though at a slightly different reduced temperature) obtained for thin films [9–12] are remained unexplained.

In this work, both XRD and SIMS analysis clearly showed the formation of MoN by N^+ ions implantation into Mo foils. The process of WN_2 formation and occurrence of a minimum in the plot of WN_2 intensity versus temperature is explained in our work [1], by considering both the residual gas behavior in the chamber and the role of substrate temperature on the residual gas reaction with W surface. We propose that the same processes may take place for N^+ implanted Mo as those for W, since all results obtained for Mo are consistent with those of W. Therefore we may explain the processes that occur during N^+ implantation of Mo, as follows: the residual gas in the chamber contains oxygen via CO, CO_2 and decomposition of water at higher temperatures explained in the following paragraph. This oxygen can react easily with the fresh Mo surface. This reaction enhances by increasing the substrate temperature, as it is well known that the oxide becomes thermodynamically more stable at higher temperatures [15–17]. In Fig. 6, the intensity of MoN for each N^+ ion energy is highest at the lowest temperature of implantation. By increasing the substrate temperature the oxide builds up on the Mo surface. In this case, when MoO_2 is in near surface layers, then the formation of MoN is thermodynamically unfavorable. This process is the cause of decreasing MoN intensity in each N^+ implantation energy and the presence of the minimum. However, this thermodynamically unfavorable reaction becomes possible when the oxide becomes a reactive sub-oxide MoO_{2-x} that results from preferential oxygen sputtering, which perhaps becomes enhanced by increasing the substrate temperature that transfers higher energy to oxygen atoms, so that their binding to Mo atoms can break more easily. The decrease of MoO_2 intensity with increasing temperature in Fig. 4(a)–(d) is a clear indication of this process. The dissociated oxygen reacts with the bombarding nitrogen ions at the surface to form Mo(N, O). With further ion implantation, Mo(N, O) gradually transforms into MoN.

The existence of oxygen in the chamber and particularly around the heated substrate holder is reported by Savaloni et al. [17], who used a quadrupole mass spectrometer and analyzed the partial pressure of the residual gas inside their UHV chamber (base pressure of 10^{-10} mbar; evaporation pressure of 10^{-8} to 10^{-7} mbar) before and after deposition of erbium as a function of substrate temperature. They reported that the substrate holder assembly is an important site for out gassing and for reactions, including those between deposited erbium and residual gases. In particular they found that water decomposes at about 600 K (see Fig. 4 in Ref. [17]). They suggested that the water and its products arise from out gassing and reactions at the substrate and substrate holder. They also related the low partial pressure of oxygen to its rapid reaction with deposited erbium. Therefore, as mentioned above there should be oxygen of different concentration (depending on the substrate temperature) around the heated sample, which can react with Mo surface to form MoO_2, which initially forms on the molybdenum surface.

It is also worth to mention that the pressure in our chamber (i.e., $\sim 10^{-5}$ mbr) is much higher than Savaloni et al.'s work [17]. Therefore, there should be much higher partial pressure for residual gases, in particular for water. Hence at high temperatures (e.g., >500 K) there should be a large amount of oxygen as a result of decomposition of water and out gassing from substrate holder assembly in the vacuum chamber.

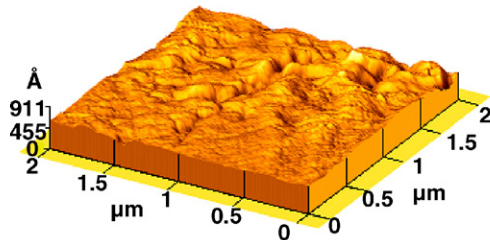

Fig. 8. AFM image of untreated molybdenum.

When the N^+ ion energy is increased the temperature for the observed minimum is also shifted to higher temperatures. This shows an interrelation between substrate temperature and the N^+ ion energy.

The crystallite size, D (coherently diffracting domains), is obtained using the Scherrer formula [18]:

$$B = \frac{k\lambda}{D\cos\theta}$$

where, λ is the wavelength of X-ray, θ the Bragg angle, and k is a dimensionless constant which is related to the shape and distribution of crystallites [19] (usually taken as unity). For obtaining the value for B, we used the usual procedure of full width half maximum (FWHM) measurement technique [20], therefore:

$$B = (W_0^2 - W_i^2)^{1/2}$$

where, W_0 is the FWHM of the sample and W_i is the FWHM of stress free sample (annealed powder sample).

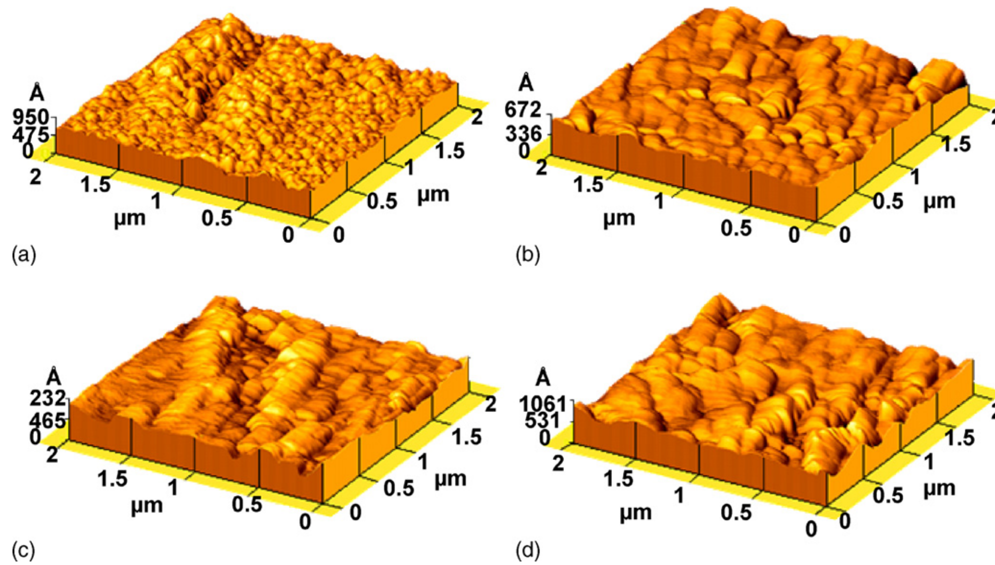

Fig. 9. AFM images of N^+ ion implanted molybdenum at 20 keV and at different final temperatures. (a) T_{sf} = 698 K; (b) T_{sf} = 725 K; (c) T_{sf} = 752 K; (d) T_{sf} = 777 K.

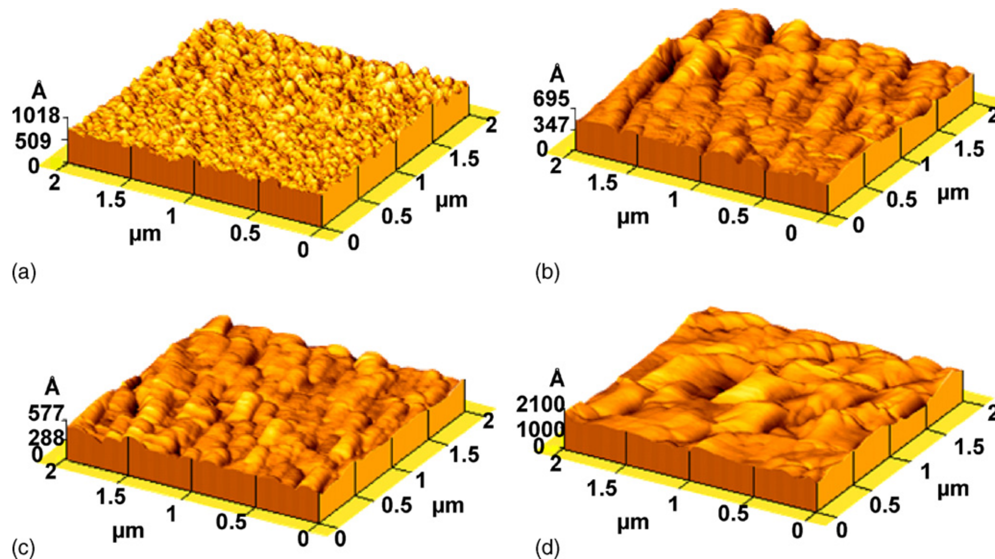

Fig. 10. AFM images of N^+ ion implanted Mo at 30 keV and at different final temperatures. (a) T_{sf} = 753 K; (b) T_{sf} = 772 K; (c) T_{sf} = 800 K; (d) T_{sf} = 833 K.

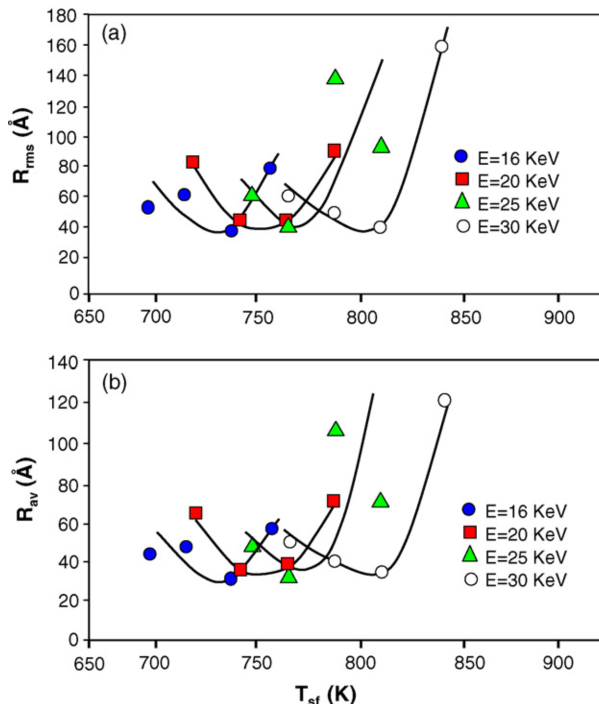

Fig. 11. (a) r.m.s. roughness and (b) average roughness of Mo samples produced at different N^+ ion energies as a function of final temperature.

The crystallite size, D (coherently diffracting domains) variation with substrate temperature obtained from MoN (0 3 1) line is given in column 7 of Table 1). The results show an increase with substrate temperature for all N^+ energies.

3.2. Surface morphologies obtained by AFM

Fig. 8 shows the surface morphology image of untreated Mo, with no clear/ordered morphology on the surface. The surface morphology images of Mo samples implanted with 20 and 30 keV N^+ ions are shown in Figs. 9(a)–(d) and 10(a)–(d) as typical examples.

Grains of columnar-like structure are formed in the surface of Mo samples produced at lowest temperature (Figs. 9(a) and 10(a)). At higher temperature (Figs. 9(b) and 10(b)), larger grains are formed and the difference between the large and small grains is still obvious. Further increase of temperature (Figs. 9(c) and (d) and 10(c) and (b)), shows a distinct change in the surface morphology. In addition, the size of the grains increases dramatically, consistent with XRD results.

Fig. 11(a) and (b) shows the r.m.s. and average roughness values obtained from AFM measurements. Both R_{rms} and R_{av} follow similar trend and consistent with microscopic observations. In general, at lowest sample temperature, the roughness has the highest value, while by increasing the temperature, due to the diffusion processes, roughness is decreased, further increase in temperature has increased the roughness. The final increase of roughness with temperature is due to grooving effect that can be seen in the higher temperature N^+ implanted samples [21–23] (Figs. 9(d) and 10(d)).

3.3. SEM electron micrographs

Similar to N^+ implanted W [1], the inadequacy of the SEM in resolving the structural changes to the degree obtained by AFM was observed. Therefore, no further discussion on SEM results is appropriate.

4. Conclusions

The surface nano-structural modifications of massive molybdenum samples (0.5 mm foils) made by nitrogen ions (of different energies and a fluence of $1 \times 10^{18}\,N^+\,cm^{-2}$) implantation are studied by SEM, XRD, AFM, and SIMS. XRD patterns clearly showed MoN (0 3 1) (hexagonal) very close to Mo (2 0 0) line. Crystallite sizes (coherently diffracting domains) obtained from MoN (0 3 1) line, showed an increase with substrate temperature. AFM images showed the formation of grains on Mo samples, which grew in size with temperature, consistent with XRD results. Similar morphological changes has been observed for N^+ implanted tungsten. The surface roughness variation with temperature initially showed a decrease with increasing temperature. Further increase of temperature increased the surface roughness which is found to be due to increasing grain size together with the grooving effect. The results of the density of implanted nitrogen ions, and the depth of nitrogen ion implantation in Mo, studied by SIMS showed a minimum for both N^+ density and depth of N^+ penetration at certain temperatures, dependent on the N^+ energy, consistent with XRD results (i.e., $I_{MoN\ (0\ 3\ 1)}$ and $I_{Mo\ (2\ 0\ 0)}/I_{Mo\ (2\ 1\ 1)}$). An explanation on the basis of residual gas, substrate temperature, dissociation of water in the chamber and the ion energy is given for the occurrence of this minimum in the results of N^+ implanted Mo and W foils.

Acknowledgements

This work was carried out with the support of the University of Tehran and the I.A. University. The authors are grateful to A. Shokohi, H. Hajhosaini, N. Shariati and P. Amiri for their assistance with ion implantation, SIMS, AFM and XRD, respectively.

References

[1] H. Savaloni, F. Modiri, Appl. Surf. Sci., in press.
[2] H.L. Zhang, D.Z. Wang, N.K. Huang, Appl. Surf. Sci. 150 (1999) 34.
[3] M. Kiuchi, Nucl. Instrum. Methods Phys. Res. B80–B81 (1993) 1343.
[4] W. Ensinger, M. Kiuchi, M. Satou, J. Appl. Phys. 77 (1995) 6630.
[5] M. Nagai, T. Miyao, Catal. Lett. 15 (1992) 105.
[6] C.W. Colling, L.T. Thompson, J. Catal. 146 (1994) 193.
[7] M.J. Ledoux, C. Pham-Huu, Catal. Lett. 15 (1992) 263.
[8] H. Savaloni, S. Bagheri Najmi, Vacuum 66 (2002) 49.
[9] H. Savaloni, M. Gholipour-Shahraki, M.A. Player, J. Phys. D: Appl. Phys. 39 (2006) 2231–2247.
[10] Z. Shi, M.A. Player, Vacuum 49 (1998) 257.
[11] H. Savaloni, A. Taherizadeh, A. Zendehnam, Physica B 349 (2004) 44.
[12] H. Savaloni, G.R. Moradi, M.A. Player, Vacuum 77 (2005) 245.
[13] D. Walton, Philos. Mag. VIII (7) (1962) 1671.

[14] D.N.J. Lee, J. Mater. Sci. 24 (1989) 4375.
[15] A.E. Curzon, J. Less Common Metals 98 (1984) 149.
[16] D.M. Holloway, W.E. Swartz Jr., Appl. Spectrosc. 31 (1977) 167.
[17] H. Savaloni, M.A. Player, G.V. Marr, Vacuum 43 (1992) 965.
[18] H. Klung, L. Alexander, X-ray Diffraction Procedure, Wiley, New York, 1954, p. 503.
[19] J.I. Langford, A.J. Wilson, J. Appl. Cryst. 11 (1978) 102.
[20] T.C. Huang, G. Lim, F. Parmigiani, E. Kay, J. Vac. Sci. Technol. A3 (1985) 2161.
[21] D.E. Aspnes, E. Kinbron, D.D. Bacon, Phys. Rev. B21 (1980) 3290.
[22] W.W. Mullins, Acta Metall. 6 (1954) 414.
[23] Z. Suo, Adv. Appl. Mech. 33 (1997) 193.